Topological phase transitions with non-Abelian gauge potentials on square lattices

Yao-Hua Chen,[*] Jian Li, and C. S. Ting

Texas Center for Superconductivity and Department of Physics, University of Houston, Houston, Texas 77204, USA
(Received 7 August 2013; published 18 November 2013)

We investigate the topological phase transition on interacting square lattices via the non-Abelian potential by employing the real-space cellular dynamical mean-field theory combining with the continuous-time Monte Carlo method. For a weak on-site Hubbard interaction, a topological band insulating state with a pair of gapless edge states is induced by a next-nearest-neighbor hopping. A phase transition from the metallic phase to the Mott insulating phase is observed when the interaction is increased. These two phases can be distinguished by detecting whether a bulk gap in the K-dependent spectral function exists. The whole phase diagrams as functions of the interaction, next-nearest-neighbor hopping energy, and temperature are presented. The experimental setup to observe these new interesting phase transitions is also discussed.

I. INTRODUCTION

The topological phases originating in spin-orbital coupling systems have attracted great attention in modern condensed matter physics.[1–5] Many interesting phenomena have been found in recent theoretical and experimental works, such as the integer and fractional quantum Hall effect, topological band insulator (TBI), topological Mott insulator, and topological superconductor.[6–17] Experimentally, the TBI has been detected in many materials, such as Bi_2Se_3 and HgTe/CdTe quantum wells.[18–25] Besides these experimental observations, there are also many theoretical proposals for simulating the TBI in systems with different geometric structures, such as honeycomb and kogome lattices.[26–28] This novel state can be identified by a gapped bulk spectrum and gapless edge states, which are protected by time-reversal symmetry. However, these previous works mainly focus on the TBI without interaction. Thus, it is desirable to investigate the influence of interactions on the TBI, which should play an important role in real systems.

One important method used to realize these exotic systems with interactions is via ultracold atoms trapped in optical lattices.[29–34] Due to the Feshbach resonance, interactions in cold atomic systems can be precisely tunedand are used to realize novel phenomena driven by strongly correlated effects, for instance, the superfluid, Mott insulator, and Fulde-Ferrell-Larkin-Ovchinnikov (FFLO) state.[35–40] However, a major disadvantage of simulating spin-orbital coupling in cold-atom systems is that charge-neutral ultracold atoms cannot be affected by external magnetic or electric fields. A recent breakthrough called artificial gauge field technology has been made to supply effective magnetic and electric fields on neutral ultracold atoms in experiments.[41,42] This new developing technology provides a crucial step to simulate spin-orbit couplings, Abelian or non-Abelian gauge fields, and, more importantly, novel topological phases in this controllable artificial system, especially the TBI.[43–47]

In this article, we investigate the band structure and topological effects in a square lattice with interaction and a non-Abelian gauge potential by employing real-space cellular dynamical mean-field theory (CDMFT) combined with the continuous-time quantum Monte Carlo (CTQMC) method. Without the on-site interaction, a gap is found near the Fermi energy, which is induced by the next-nearest-neighbor

(NNN) hopping t'. Two edge states are observed from the energy dispersion. When the interaction increases, the bulk gap is closed and edge states disappear. This gapless behavior suggests that the system becomes a paramagnetic metal (PM). When the interaction is stronger than the critical interaction U_c, a big gap can be found near the Fermi energy. This indicates a phase transition from a metallic state into a paramagnetic Mott insulator (PMI) state. In addition, a collinear antiferromagnetic order is formed when the temperature is lower than the Curie temperature, and the double occupancy is gradually suppressed as the interaction increases.

This paper is constructed as follows. The model Hamiltonian and method are introduced in Sec. II. In Sec. III, we investigate the noninteraction case and find that the ground state of the system is a TBI. The interaction effects on the TBI are presented in Sec. IV. We present the phase diagrams in Sec. V. In Sec. VI, we discuss the experimental setup to realize our system and the relevant physics. Section VI presents a summary and discussion.

II. MODEL AND METHOD

We consider the standard Hubbard model on a half-filling square lattice in the presence of a non-Abelian gauge potential,

$$H = -t \sum_{\langle ij \rangle \sigma\sigma'} c_{i\sigma}^+ T_{ij}^{\sigma\sigma'} c_{j\sigma'} - t' \sum_{\langle\langle ij \rangle\rangle \sigma\sigma'} c_{i\sigma}^+ T'^{\sigma\sigma'}_{ij} c_{j\sigma'} + \text{H.c.}$$
$$+ U \sum_i n_{i\uparrow} n_{i\downarrow} + \mu \sum_{i\sigma} n_{i\sigma}, \qquad (1)$$

where t is the nearest-neighbor hopping energy [see lighter (red) arrows in Fig. 1(a)], t' is the NNN hopping energy [see (blue) arrows in Fig. 1(b)], U is the on-site repulsive interaction, and μ is the chemical potential, which keeps the system at half-filling. $c_{i\sigma}^+$ and $c_{i\sigma}$ denote the creation and annihilation operators, respectively, and $n_{i\sigma} = c_{i\sigma}^+ c_{i\sigma}$ corresponds to the density operator. $T_{ij}^{\sigma\sigma'}$ can be written as $T_{ij} = T_x = e^{i\psi_1 \sigma_x}$ and $T_y = e^{i\psi_2 \sigma_y}$, which corresponds to the flux induced by the nearest-neighbor hopping. $T'^{\sigma\sigma'}_{ij}$ can be written as $T'_1 = e^{i\psi'_1 \sigma_x}$ [see direction 1 in Fig. 1(b)] and $T'_2 = e^{i\psi'_2 \sigma_y}$ [see direction 2 in Fig. 1(b)]. Here, we use $\psi_1 = \psi_2 = \psi'_1 = \psi'_2 = \pi/4$ and $t = 1.0$, which is also set as
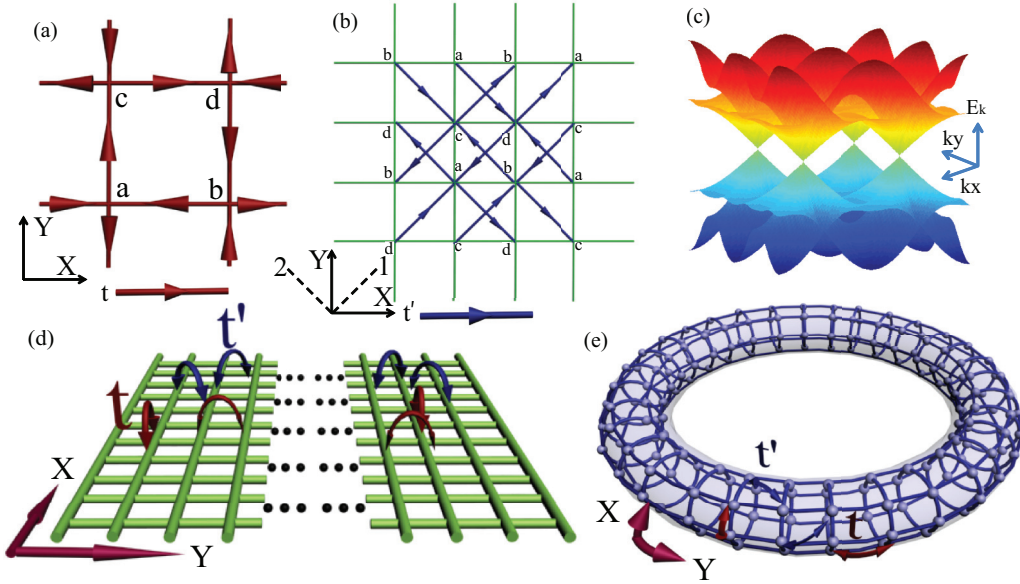
FIG. 1. (Color online) (a) Sketch of a square lattice via a non-Abelian gauge potential; lighter (red) arrows show the nearest-neighbor hopping t. (b) Next-nearest-neighbor hopping t' in a square lattice with a non-Abelian gauge potential is denoted by (blue) arrows. Dashed lines indicate the direction of T'_1 and T'_2. (c) Energy band structure when $t' = 0$ without interaction. There are four Dirac points, near the $(\frac{\pi}{2}, \frac{\pi}{2})$, $(\frac{\pi}{2}, -\frac{\pi}{2})$, $(-\frac{\pi}{2}, \frac{\pi}{2})$, and $(-\frac{\pi}{2}, -\frac{\pi}{2})$ point. (d, e) Schematic of a system with (d) open boundary conditions and (e) periodic boundary conditions.

the energy unit. Figure 1(c) shows the energy band structure when $t' = 0$ and $U = 0$. Four Dirac points can be found, near $(\frac{\pi}{2}, \frac{\pi}{2})$, $(\frac{\pi}{2}, -\frac{\pi}{2})$, $(-\frac{\pi}{2}, \frac{\pi}{2})$, and $(-\frac{\pi}{2}, -\frac{\pi}{2})$, which is similar to the spectrum of the honeycomb lattice. Figures 1(d) and 1(e) show two systems, with open and periodic boundary conditions, respectively, in which the lighter (red) arrows represent nearest-neighbor hopping and the darker (blue) arrows denote NNN hopping. For the open boundary case, there are N_L sites along the Y axis, while a square lattice is used in the periodic boundary case. The latter case is equivalent to a big circular loop, as shown in Fig. 1(e).

We use real-space CDMFT combined with CTQMC to investigate the interaction effects on this system, which is developed in the framework of the real-space DMFT.[48–53] The real-space DMFT has been used to investigate phase transitions driven by interactions in systems without periodic boundary conditions, such as investigating the metal–Mott insulator phase transition in a three-dimensional optical lattice with an exterior magnetic field.[34,54,55] However, this method works ineffectively in low-dimensional systems due to the ignoring of nonlocal correlation and spatial fluctuations. Therefore, the real-space CDMFT is developed to incorporate spatially extended correlations and geometrical frustration by mapping the original lattice to many clusters embedded in effective media. We use CTQMC[56,57] as an impurity solver, which is more accurate than the traditional QMC method due to the absence of Trotter decomposition. This new method has been used to investigate the competion of interaction and topological effect on a honeycomb lattice.[27]

In the real-space CDMFT, the original lattice is mapped to N_c clusters embedded in effective media. There are N_s sites in every cluster. The whole lattice has $N_{all} = N_c \times N_s$ sites. A self-consistent loop can be started by guessing the

self-energy $\hat{\Sigma}$. Then the real-space CDMFT coarse-grained Green's function $\hat{G}$ is obtained by $\hat{G} = \frac{1}{N_k} \sum_k \frac{1}{i\omega_n - \mu - \hat{t}(k) - \hat{\Sigma}}$. The Weiss field function, gotten by the Dyson equation $\hat{g}^{-1} = \hat{G}^{-1} + \hat{\Sigma}$, is used as the input of the impurity solver CTQMC. We recalculate the self-energy $\hat{\Sigma}$ by $\hat{\Sigma} = \hat{g}^{-1} + \hat{G}_{is}^{-1}$ to finish the iterative loop, where $\hat{G}_{is}$ is the new Green's function given by the impurity solver CTQMC. The real-space CDMFT self-consistent iterative loop is repeated until it converges with the self-energy $\hat{\Sigma}$. Then the physical property is obtained by other codes, such as double occupancy and magnetism. The K-dependent spectral function $A(\vec{k}, \omega)$ can be gotten by the maximum entropy method,[58] and the density of states (DOS) is given by $\rho(\omega) = \frac{1}{N_k} \Sigma_{\vec{k}} A(\vec{k}, \omega)$, which describes the number of states at frequency ω.

III. TOPOLOGICAL BAND INSULATING PHASE IN A NONINTERACTING SYSTEM

The energy band structures without interaction for different NNN hoppings t' are shown in Fig. 2. Figures 2(a) and 2(b) show the bulk energy band structures obtained under the periodic boundary condition. With $t' = 0$, we find that the up-band touches the down-band near the Fermi energy, as shown in Fig. 2(a). An obvious gap induced by the NNN hopping t' is found near the Fermi energy at $t' = 0.5$ [see Fig. 2(b)]. The energy band structure obtained under the open boundary condition is shown in Figs. 2(c) and 2(d). Differently from the periodic boundary case, the system is a band insulator even at $t' = 0$. As shown in Fig. 2(c), a small visible gap is observed in the spectrum. When we increase t' to 0.5, a pair of edge states appears close to the $\pi/2$ point, as shown in Fig. 2(d).
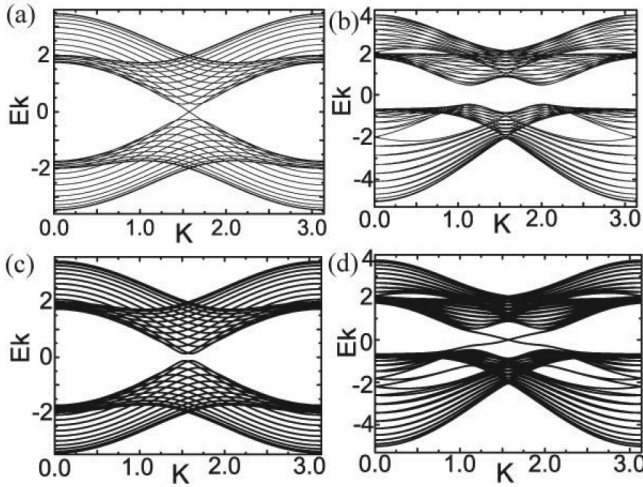
FIG. 2. Energy band structure without interaction at different next-nearest-neighbor hoppings t' when $N_L = 20$. Bulk energy band structure obtained under periodic boundary conditions [see Fig. 1(e)] with (a) $t' = 0$ and (b) $t' = 0.5$. Energy band structure obtained under open boundary conditions [see Fig. 1(d)] with (c) $t' = 0$ and (d) $t' = 0.5$.

This indicates that the TBI phase induced by t' appears at $t' = 0.5$.

IV. INTERACTION EFFECTS

In this section, we take the on-site Hubbard interaction into consideration and show how the interaction U affects the phases discussed above. To observe the interaction effects, we present the spectral function for different U values with $t' = 0.5$ in Fig. 3. Figures 3(a)–3(c) show the K-dependent spectral functions for different interactions U with the temperature $T = 0.4$, which are obtained from the periodic boundary condition. When $U = 1.0$, a bulk insulating gap can be found near the Fermi energy, which is induced by NNN hopping with the non-Abelian potential [see Fig. 3(a)]. This gap is closed by tuning the interaction to $U = 3.0$ [see Fig. 3(b)], indicating a transition from a gapped insulating state to a gapless metallic state. As U becomes stronger than the critical interaction $U_c^{\text{PM-PMI}} = 10.9$ at $T = 0.4$, we find that the insulating gap is reopened [see Fig. 3(c)], implying a transition from a metallic state to an insulating state. Figures 3(d) and 3(e) exhibit the K-dependent spectral functions for the open boundary condition at $T = 0.4$ for various U's. The edge states connecting the up-band and down-band are shown in Fig. 3(d), which means that the system becomes a TBI at $U = 1.0$. The edge states disappear at $U = 14.0$, and a large Hubbard gap can be seen near the Fermi energy, as shown in Fig. 3(e). The evolution of the bulk DOS at $T = 0.2$ is shown in Fig. 3(f). Gapped-gapless-gapped behavior is found in the bulk DOS when the interaction increases, indicating that the system undergoes a TBI–metal insulator phase transition.

Figure 4(a) shows the evolution of a single-particle gap ΔE in the bulk obtained from the DOS as a function of U for $t' = 0.5$ and $T = 0.2$ and 0.4. To determine whether there are magnetic transitions during the process of increasing U, we also present the ferromagnetic magnetization intensity m,
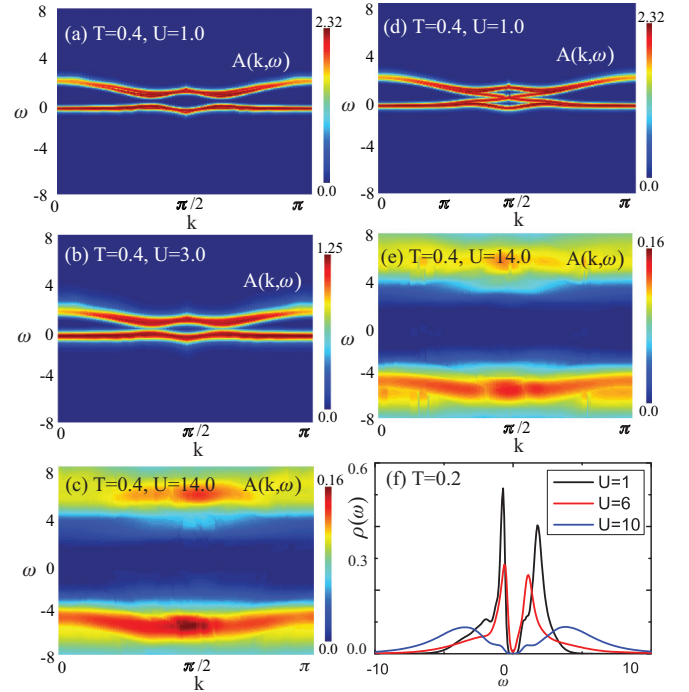

FIG. 3. (Color online) Evolution of the K-dependent spectral function $A(k,\omega)$ and density of states on different U's with $t' = 0.5$. $A(k,\omega)$ obtained under periodic boundary conditions with (a) $T = 0.4$, $U = 1.0$, (b) $T = 0.4$, $U = 3.0$, and (c) $T = 0.4$, $U = 14.0$. $A(k,\omega)$ obtained under open boundary conditions with (d) $T = 0.4$, $U = 1.0$ and (e) $T = 0.4$, $U = 14.0$. (f) Evolution of the bulk density of state $\rho(\omega)$ at various interactions U with $T = 0.2$.

staggered magnetization intensity ms, and collinear antiferromagnetic order parameter ms' in Fig. 4. Here m is defined as $m = \frac{1}{N}\sum_i^N (n_{i\uparrow} - n_{i\downarrow})$, and it describes the ferromagnetic order [see Fig. 4(b)]. The staggered magnetization intensity ms [see Fig. 4(c)] is obtained by $ms = \frac{1}{N}\sum_i^N \text{sign}(i)(n_{i\uparrow} - n_{i\downarrow})$, where $\text{sign}(i) = +1$ with $i = a,d$, and $\text{sign}(i) = -1$ with $i = b,c$. Points a–d are defined in Fig. 1(a). The collinear antiferromagnetic order [see Fig. 4(d)] can be identified by a new order parameter, ms', which is defined by $ms' = \frac{1}{N}\sum_i^N \text{sign}'(i)(n_{i\uparrow} - n_{i\downarrow})$, where $\text{sign}'(i) = +1$ with $i = a,b$ and $\text{sign}'(i) = -1$ with $i = c,d$. In Fig. 4(a), we find that the gap is opened up at $T = 0.2$ by the NNN hopping term t', and it decreases when U increases as long as $U < 5.2$. As the interaction becomes stronger than the critical interaction $U_c^{\text{TBI-PM}} = 5.2$, the gap is closed. This gapless behavior indicates that the system stays in a metallic state. The interaction-induced insulating state is found when $U > U_c^{\text{PM-PMI}} = 10.9$. A gap is reopened near the Fermi energy. The parameters m, ms, and ms' are all nearly 0 when the interaction increases, and this means that no magnetic order exists. The critical point of the interaction in the TBI-metal transition decreases when the temperature increases [see inset in Fig. 4(a)]. This indicates that the TBI is more stable at low temperatures due to the suppression of thermodynamic fluctuations. Figure 5 shows the evolution of m, ms, and ms' as a function of T for $t' = 0.5$, $U = 12.0$. It is found that ms' increases to a finite value, while m and ms remain nearly 0 with $T < T_{\text{Curie}} \approx 0.19$. This implies that there is a phase transition from the PMI to the
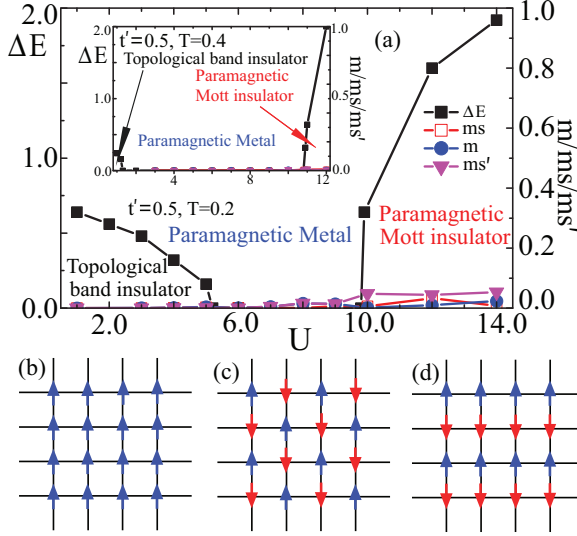
FIG. 4. (Color online) (a) Development of the single-particle gap ΔE, magnetization intensity m, staggered magnetization intensity ms, and collinear antiferromagnetic order parameter ms' as a function of interaction U at $t' = 0.5$, with $T = 0.2$ and $T = 0.4$ (inset). Sketches of (b) ferromagnetic order, (c) antiferromagnetic order, and (d) collinear antiferromagnetic order.

collinear antiferromagnetic insulating phase as T is lowered below the Curie temperature, indicating that the PMI state is not a spin-liquid state.[59,60]

The evolution of double occupancy $D_{occ} = \frac{\partial F}{\partial U} = \frac{1}{N}\sum_i^N \langle n_{i\uparrow} n_{i\downarrow}\rangle$ as a function of the interaction for different T's when $t' = 0.5$ is shown in Fig. 6(a). The arrows show the critical points of the metal–Mott insulator transition at different T values. At $U < U_c^{PM-PMI}$, the double occupancy increases due to the suppression of thermodynamic fluctuations of particles by the decreasing T. The double occupancy remains small at $U > U_c^{PM-PMI}$, and this suggests that the system is just singly occupied when the interaction is strong enough. The low double occupancy means that the system becomes a Mott insulator, in which there is only one particle at one site with half-filling. We also find that the double occupancies at different T values are almost suppressed at $U > U_c^{PM-PMI}$. This indicates that T does not affect the itinerancy of particles when the metal–Mott insulator phase translation
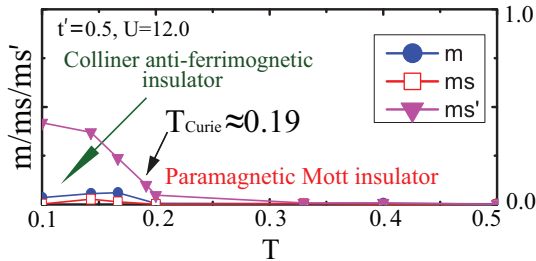

FIG. 5. (Color online) Evolutions of ferromagnetic magnetization intensity m, staggered magnetization intensity ms, and collinear antiferromagnetic order parameter ms' as a function of temperature T at $t' = 0.5$ and $U = 12.0$. The black arrow indicates the Curie temperature.
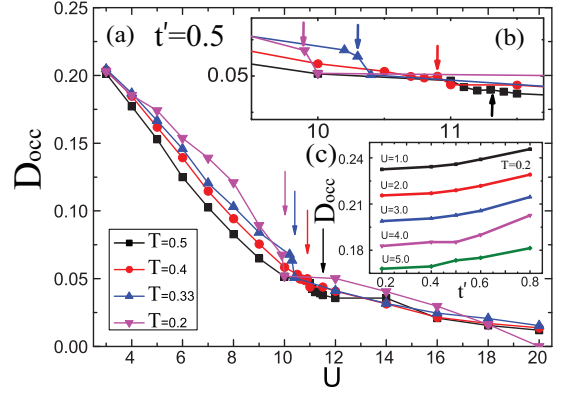

FIG. 6. (Color online) (a) Evolution of double occupancy D_{occ} as a function of U for different T values with $t' = 0.5$. Arrows show the critical points of the metal–Mott insulator transition at different T values. (b) Magnification of the double occupancy near the critical point. (c) Evolution of double occupancy as a function of t' for different U values with $T = 0.2$.

occurs. D_{occ} decreases smoothly as U is increased. However, a discontinuous decreasing behavior is found near the critical point [see Fig. 6(b)], which is obvious at low temperatures and suggests that the metal–Mott insulator phase transition is a first-order phase transition.[61,62] Figure 6(c) shows the evolution of double occupancy as a function of t' at different U values with $T = 0.2$. The double occupancy increases when t' is increased due to the enhancement of the itinerancy of the particles.

V. PHASE DIAGRAM

The phase diagrams in terms of the interaction U, temperature T, and NNN hopping t' with a non-Abelian gauge potential are plotted in Fig. 7. The black line represents the phase boundary between PM and PMI, where the diamonds exhibit the critical interaction U_c^{PM-PMI}. The phase boundary between TBI and PM is illustrated by the (red) line with squares (indicating U_c^{TBI-PM}). Figure 7(a) shows the U-T phase diagram at $t' = 0.5$. The TBI induced by t' is broken when U is increased, and a PM state emerges. The PMI induced by U can be seen at $U > U_c^{PM-PMI}$. The critical interaction U_c^{TBI-PM} increases when the temperature decreases, which shows that the TBI state is more stable at low temperatures due to the suppression of thermodynamic fluctuations. Figure 7(b) shows the U-t' phase diagram at $T = 0.2$. The system undergoes a PM-PMI transition driven by U at $t' = 0$. The TBI phase can be seen when t' is strong, such as at $t' > 0.1$. It is destroyed by the interaction, and PM can be found at $U > U_c^{TBI-PM}$. When the interaction is stronger than the critical interaction U_c^{PM-PMI}, a gap can be reopened near the Fermi energy, indicating a PM-PMI transition.

VI. EXPERIMENTAL SETUP

The topological-insulator and Mott-insulator transition induced by the interaction U can be realized by the newly developed laser-induced-gauge-field method in a cold-atom system.[41,42] In Fig. 8(a), we show a sketch of experimental setup to form a square lattice with NNN hopping, which is
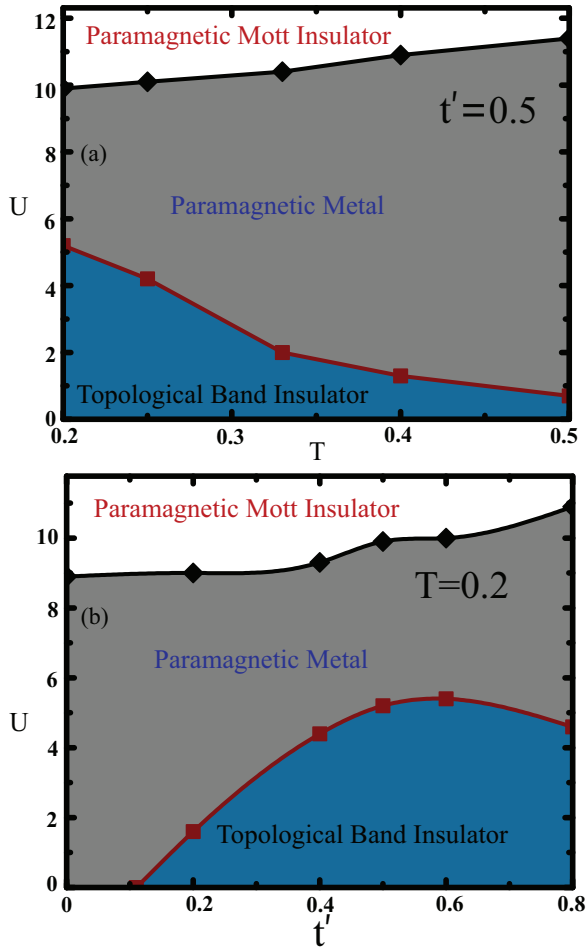
FIG. 7. (Color online) Phase diagrams as a function of U, T, and t'. The black line with diamonds shows the phase boundary between a paramagnetic Mott insulator (white area) and a paramagnetic metal (gray area). The phase boundary between the paramagnetic metal and the topological band insulator (blue area) is shown by the (red) line with squares. (a) U-T phase diagram with $t' = 0.5$. (b) U-t' phase diagram with $T = 0.2$.

similar to that producing a honeycomb optical lattice.[63] Four retroreflected laser beams are used to construct two square lattices, A and B, coexisting on the same plane. Raman laser beams are employed to produce the hopping t_{ab}, as well as to create and adjust the phase ψ with hopping terms. The lattice structure is shown in Fig. 8(b). Specifically, the hopping amplitudes satisfy $t_a = t_b \equiv t'$ and $t_{ab} \equiv t$.

After the square lattice and the non-Abelian gauge potential are established, we can fill this system with cold atoms, such as ^{40}K. With the help of Feshbach resonance, the interaction
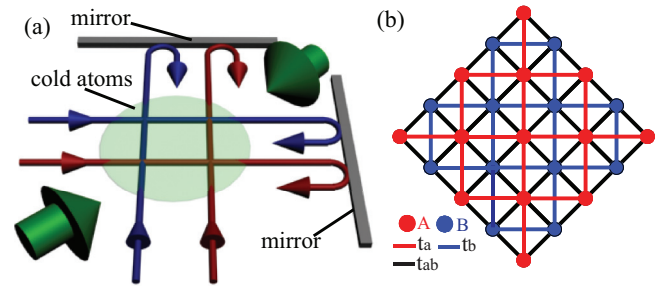

FIG. 8. (Color online) (a) Sketch of the experimental setup to form a square lattice with next-nearest-neighbor hopping. Red and blue lines with arrows denote retroreflected laser beams, which create two square lattices. Raman laser beams are shown by green lines with arrows. The gray cuboid indicates mirrors, and cold atoms are signified by the light-green oval. (b) Lattice structure: A [lighter (red) circles] and B [darker (blue) circles] are two square lattices created by retroreflected laser beams. Hopping between A and B induced by Raman laser beams is shown by black lines.

between these atoms can be accurately controlled, which facilitates observation of the phenomena we are proposing. To detect the topological structures, one can use the semiclassical wave-packet dynamics or time-of-flight method.[63,64] The latter method can also be used to detect the double occupancy of the system and to confirm whether the system is a Mott insulator.[37]

VII. SUMMARY

In summary, we have obtained the phase diagrams of interacting square lattices via the non-Abelian potential by employing real-space CDMFT combined with the CTQMC method. The TBI induced by the NNN hopping t' is found when the interaction is weak. Increasing the interaction can break the topological state, and a gapless PM state appears at $U_c^{\text{TBI-PM}} U < U < U_c^{\text{PM-PMI}}$. As the interaction $U > U_c^{\text{PM-PMI}}$, a gapped PMI state occurs. The system undergoes a transition from a PMI state to a collinear antiferrimagnetic insulating state at $T < T_{\text{Curie}}$. We also present the K-dependent spectral functions and double occupancy, which may be detected in future experiments. Our studies provide a helpful step toward understanding the stability of the TBI state under the effects of interaction, temperature, and different NNN hoppings.

*chenyaohua23@gmail.com

[1]C. L. Kane and E. J. Mele, Phys. Rev. Lett **95**, 146802 (2005).

[2]C. L. Kane and E. J. Mele, Phys. Rev. Lett **95**, 226801 (2005).

[3]M. Z. Hasan and C. L. Kane, Rev. Mod. Phys **82**, 3045 (2010).

[4]X. L. Qi and S. C. Zhang, Rev. Mod. Phys **83**, 1057 (2010).

[5]C. Z. Chang, J. S. Zhang, X. Feng, J. Shen, Z. C. Zhang, M. H. Guo, K. Li, Y. B. Ou, P. Wei, L. L. Wang, Z. Q. Ji, Y. Feng, S. H. Ji, X. Chen, J. F. Jia, X. Dai, Z. Fang, S. C. Zhang, K. He, Y. Y. Wang, L. Lu, X. C. Ma, and Q. K. Xue, Science **340**, 167 (2013).

[6] H. J. Zhang, C. X. Liu, X. L. Qi, X. Dai, Z. Fang, and S. C. Zhang, Nature Phys. **5**, 438 (2009).

[7] Z. Liu, E. J. Bergholtz, H. Fan, and A. M. Läuchli, Phys. Rev. Lett **109**, 186805 (2012).

[8] H. Z. Lu, J. R. Shi, and S. Q. Shen, Phys. Rev. Lett **107**, 076801 (2011).

[9] D. Xiao, W. Yao, and Q. Niu, Phys. Rev. Lett. **99**, 236809 (2007).

[10] S. Raghu, X. L. Qi, C. Honerkamp, and S. C. Zhang, Phys. Rev. Lett **100**, 156401 (2008).

[11] R. Yu, W. Zhang, H. J. Zhang, S. C. Zhang, X. Dai, and Z. Fang, Science **329**, 5987 (2010).

[12] M. Kargarian and G. A. Fiete, Phys. Rev. B **82**, 085106 (2010).

[13] K. Nomura, S. Ryu, A. Furusaki, and N. Nagaosa, Phys. Rev. Lett **108**, 026802 (2012).

[14] K. Sun, W. V. Liu, A. Hemmerich, and S. D. Sarma, Nature Phys. **8**, 67 (2012).

[15] Y. J. Wu, J. He, C. L. Zang, and S. P. Kou, Phys. Rev. B **86**, 085128 (2012).

[16] J. He, Y. Liang, and S. P. Kou, Phys. Rev. B **85**, 205107 (2012).

[17] Y. F. Jia, H. M. Guo, Z. Y. Chen, S.-Q. Shen, and S. P. Feng, Phys. Rev. B **88**, 075101 (2013).

[18] B. A. Bernevig, T. L. Hughes, and S. C. Zhang, Science **314**, 1757 (2006).

[19] D. Hsieh, D. Qian, L. Wray, Y. Xia, Y. S. Hor, R. J. Cave, and M. Z. Hasan, Nature **452**, 970 (2008).

[20] Y. L. Chen, J. G. Analytis, J. H. Chu, Z. K. Liu, S. K. Mo, X. L. Qi, H. J. Zhang, D. H. Lu, X. Dai, Z. Fnag, S. C. Zhang, I. R. Fisher, Z. Hussain, and Z. X. Shen, Science **325**, 178 (2009).

[21] Y. Xia, D. Qian, D. Hsieh, L. Wray, A. Pal, H. Lin, A. Bansil, D. Grauer, Y. S. Hor, R. J. Cava, and M. Z. Hasan, Nature Phys. **5**, 398 (2009).

[22] S. Chadov, X. L. Qi, J. Kübler, G. H. Fecher, C. Felser, and S. C. Zhang, Nat. Mater. **9**, 541 (2010).

[23] K. Kuroda, M. Arita, K. Miyamoto, M. Ye, J. Jiang, A. Kimura, E. E. Krasovskii, E. V. Chulkov, H. Iwasawa, T. Okuda, K. Shimada, Y. Ueda, H. Namatame, and M. Taniguchi, Phys. Rev. Lett **105**, 076802 (2010).

[24] H. J. Zhang, S. Chadov, L. Müchler, B. H. Yan, X. L. Qi, J. Kübler, S. C. Zhang, and C. Felser, Phys. Rev. Lett **106**, 156402 (2011).

[25] Z. H. Pan, E. Vescovo, A. V. Fedorov, D. Gardner, Y. S. Lee, S. Chu, G. D. Gu, and T. Valla, Phys. Rev. Lett. **106**, 257004 (2011).

[26] D. Cocks, P. P. Orth, S. Rachel, M. Buchhold, K. Le Hur, and W. Hofstetter, Phys. Rev. Lett. **109**, 205303 (2012).

[27] W. Wu, S. Rachel, W. M. Liu, and K. Le Hur, Phys. Rev. B **85**, 205102 (2012).

[28] G. Go, J. H. Park, and J. H. Han, Phys. Rev. B **87**, 155112 (2013).

[29] D. Jaksch, C. Bruder, J. I. Cirac, C. W. Gardiner, and P. Zoller, Phys. Rev. Lett. **81**, 3108 (1998).

[30] W. Hofstetter, J. I. Cirac, P. Zoller, E. Demler, and M. D. Lukin, Phys. Rev. Lett. **89**, 220407 (2002).

[31] L. Santos, M. A. Baranov, J. I. Cirac, H. U. Everts, H. Fehrmann, and M. Lewenstein, Phys. Rev. Lett. **93**, 030601 (2004).

[32] D. Joksch and P. Zoller, Ann. Phys. (N.Y.) **315**, 52 (2005).

[33] I. Bloch, J. Dalibard, and W. Zwerger, Rev. Mod. Phys. **80**, 885 (2008).

[34] U. Schneider, L. Hackermller, S. Will, Th. Best, I. Bloch, T. A. Costi, R. W. Helmes, D. Rasch, and A. Rosch, Scienc **322**, 1520 (2009).

[35] M. Greiner, O. Mandel, T. Esslinger, T. W. Hänsch, and I. Bloch, Nature (London) **415**, 39 (2002).

[36] Y. Shin, C. H. Schunck, A. Schirotzek, and W. Ketterle, Nature (London) **451**, 689 (2008).

[37] R. Jördans, N. Strohmaier, K. Günter, H. Moritz, and T. Esslinger, Nature (London) **455**, 204 (2008).

[38] N. Gemelke, X. Zhang, C. L. Hung, and C. Chin, Nature (London) **460**, 995 (2009).

[39] J. Li, J. An, and C. S. Ting, Phys. Rev. Lett. **109**, 196402 (2012).

[40] M. C. Beeler, R. A. Williams, K. Jiménez-Garcia, L. J. LeBlanc, A. R. Perry, and I. B. Spielman, Nature (London) **498**, 201 (2013).

[41] N. Goldman, I. Satija, P. Nikolic, A. Bermudez, M. A. Martin-Delgado, M. Lewenstein, and I. B. Spielman, Phys. Rev. Lett. **105**, 255302 (2010).

[42] P. Wang, Z. Q. Yu, Z. Fu, J. Miao, L. Huang, S. Chai, H. Zhai, and J. Zhang, Phys. Rev. Lett. **109**, 095301 (2012).

[43] K. Osterloh, M. Baig, L. Santos, P. Zoller, and M. Lewenstein, Phys. Rev. Lett. **95**, 010403 (2005).

[44] N. Goldman, A. Kubasiak, A. Bermudez, P. Gaspard, M. Lewenstein, and M. A. Martin-Delgado, Phys. Rev. Lett. **103**, 035301 (2009).

[45] A. M. Dudarev, R. B. Diener, I. Carusotto, and Q. Niu, Phys. Rev. Lett. **92**, 153005 (2004).

[46] P. Hauke, O. Tieleman, A. Celi, C. Ölschläger, J. Simonet, J. Struck, M. Windpassinger, K. Sengstock, M. Lewenstein, A. Eckardt *et al.*, Phys. Rev. Lett **109**, 145301 (2012).

[47] F. D. Sun, X. L. Yu, J. W. Ye, H. Fan, and W. M. Liu, Sci. Rep. **3**, 2119 (2013).

[48] A. Georges, G. Kotliar, W. Krauth, and M. J. Rozengerg, Rev. Mod. Phys. **68**, 13 (1996).

[49] O. Parcollet, G. Biroli, and G. Kotliar, Phys. Rev. Lett. **92**, 226402 (2004).

[50] T. Maier, M. Jarrell, T. Pruschke, and M. H. Hettler, Rev. Mod. Phys. **77**, 1027 (2005).

[51] G. Kotliar, S. Y. Savrasov, K. Haule, V. S. Oudovenko, O. Parcollet, and C. A. Marianetti, Rev. Mod. Phys. **78**, 865 (2006).

[52] H. Park, K. Haule, and G. Kotliar, Phys. Rev. Lett. **101**, 186403 (2008).

[53] L. DeLeo, M. Civelli, and G. Kotliar, Phys. Rev. Lett. **101**, 256404 (2008).

[54] R. W. Helmes, T. A. Costi, and A. Rosch, Phys. Rev. Lett. **100**, 056403 (2008).

[55] E. V. Gorelik, I. Titvinidze, W. Hofstetter, M. Snoek, and N. Blümer, Phys. Rev. Lett. **105**, 065301 (2010).

[56] A. N. Rubtsov, V. V. Savkin, and A. I. Lichtenstein, Phys. Rev. B **72**, 035122 (2005).

[57] E. Gull, A. J. Millis, A. I. Lichtenstein, A. N. Rubtsov, M. Troyer, and P. Werner, Rev. Mod. Phys. **83**, 349 (2011).

[58] M. Jarrell and J. E. Gubernatis, Phys. Rep. **269**, 133 (1996).

[59] P. A. Lee, N. Nagaosa, and X. G. Wen, Rev. Mod. Phys. **78**, 17 (2006).

[60] L. Balents, Nature (London) **464**, 199 (2010).

[61] T. Ohashi, N. Kawakami, and H. Tsunetsugu, Phys. Rev. Lett. **97**, 066401 (2006).

[62] T. Yoshioka, A. Koga, and N. Kawakami, Phys. Rev. Lett. **103**, 036401 (2009).

[63] E. Alba, X. Fernandez-Gonzalvo, J. Mur-Petit, J. K. Pachos, and J. J. Garcia-Ripoll, Phys. Rev. Lett. **107**, 235301 (2011).

[64] H. M. Price and N. R. Cooper, Phys. Rev. A **85**, 033620 (2012).